Chimica Techno Acta
published by Ural Federal University
eISSN 2411-1414
chimicatechnoacta.ru

ARTICLE
2023, vol. 10(3), No. 202310313
DOI: 10.15826/chimtech.2023.10.3.13

Synthesis of highly-porous nitrogen-doped carbon materials by pyrolysis of melamine-formaldehyde resin using a hard template

Yuliya Sinelnikova [ab *], Alexander Nizovskii [c], Nikolai Uvarov [ab]

a: Novosibirsk State Technical University, Novosibirsk 630073, Russia
b: Institute of Solid State Chemistry and Mechanochemistry, Siberian Branch of the Russian Academy of Sciences, Novosibirsk 630090, Russia
c: Boreskov Institute of Catalysis, Siberian Branch of the Russian Academy of Sciences, Novosibirsk 630090, Russia
* Corresponding author: yu.sinelnikova.2014@stud.nstu.ru

This paper belongs to the RKFM'23 Special Issue: https://chem.conf.nstu.ru/.
Guest Editors: Prof. N. Uvarov and Prof. E. Aubakirov.

Abstract

The use of nitrogen-doped carbon materials as electrodes in supercapacitors is a promising area of research. In this study highly-porous nitrogen-containing carbon materials were obtained by pyrolysis of melamine formaldehyde resin in the presence of nanocrystalline MgO as a hard template that was washed off after the pyrolysis. Magnesium citrate was used as a precursor for the synthesis of the template agent in situ during the pyrolysis of the resin. The obtained materials were characterized by X-ray diffraction, BET nitrogen adsorption method and Raman spectroscopy. The presence of nitrogen in the amount of 4 atomic percent was proved by XPS spectroscopy. The specific surface area was found to increase monotonically from 10 to 1300 m^2/g with an increase in the content of magnesium citrate in the initial mixture. The samples showed high capacitance of 120 F/g in 1 M H_2SO_4 electrolyte and can be used in supercapacitors.

Keywords

nitrogen-doped carbon materials
template synthesis
hard template
highly-porous carbon electrode materials
supercapacitors

Received: 28.08.23
Revised: 29.09.23
Accepted: 29.09.23
Available online: 04.10.23

Key findings

- Nitrogen doped carbon materials were obtained by pyrolysis of melamine formaldehyde resin with the addition of a hard template agent. As a template agent, nanocrystalline magnesium oxide was used, which was obtained by in situ thermolysis of magnesium citrate.
- The hard template method allowed obtaining carbon materials containing 4 at.% of nitrogen having a specific surface area up to 1300 m^2/g with a high yield of the product.
- The materials have a high specific capacitance values mainly due to the pseudocapacitance ranging from 10–120 F/g in an acidic electrolyte to 3–65 F/g in an alkaline electrolyte.

1. Introduction

Among all advanced devices for the electric energy accumulation, supercapacitors are of interest due to their unique properties, such as a high power density, fast charge-discharge, a large number of cycles and a high charge retention [1]. Carbon materials such as carbon nanotubes [2], graphene [3, 4], activated carbon [5], mesoporous carbon [6], carbon fibres [7, 8], carbon nanosheets [9, 10], etc., are promising electrode materials for space charge storage as electrodes in supercapacitors. Despite all the mentioned advantages of supercapacitors, they have a relatively low energy density compared to other electrochemical devices. One of the solutions to this problem is an increase in the specific capacity of electrode materials. It is possible by increasing the specific surface area and the number of mesopores, as well as introducing additional functional groups on the surface of the electrodes. In the literature, there are studies on modification of the surface of a carbon material with sulfur [11–13], nitrogen [14, 15], phosphorus [16, 17] and boron [18, 19] atoms.

It is also known that alloying carbon materials with nitrogen atoms increases their charge capacity. This effect can be explained by the presence of nitrogen-containing functional groups on the carbon surface, which increases the capacity of the electrodes through redox reactions [20].

Also, the introduction of nitrogen increases the wettability of the carbon material due to increasing the hydrophilicity of the pores, which enhances the capacity of the electric double layer (EDL) due to an increase in the concentration of electrolyte ions [21], and also improves the contact at the electrode/electrolyte interface along with a decrease in resistance [22]. Doping of the electrode carbon material with nitrogen allows supercapacitors with EDL to work in aqueous electrolytes, which is a promising approach for expanding the application area of these supercapacitors. Working in aqueous electrolytes makes supercapacitors safer, more affordable and increases their operation time.

In the literature, there are two main approaches to the preparation of nitrogen-containing carbon materials: the introduction of nitrogen on the surface of the material by heat treatment with nitrogen-containing gases [23, 24] and the introduction of nitrogen into the material by carbonization of nitrogen-containing precursors [25, 26].

Cui et al. [27] described a method for obtaining melamine-formaldehyde resins (MFR) in various solvents and with various ratios of initial components without the use of a template agent. In their work the authors obtained samples with the maximum specific surface area of 1000 m^2/g and large pores, which allowed them to regard such carbon materials as adsorbents. The synthesis of carbon material and, both undoped and doped with nitrogen, as well as the comparative characteristics of the obtained samples was reported in the paper [28]. Aniline was used as a source of nitrogen in this work. Electrochemical studies of the materials obtained showed that carbon doped with nitrogen has higher electrochemical capacitance properties than the carbon material itself. The specific capacitances of carbon and carbon doped with nitrogen were 13.56 and 192.12 F/g at a current density of 1 A/g, which means that doping with nitrogen makes it possible to increase the capacitive characteristics by a factor of 14. Liu et al. [29] reported the synthesis of nitrogen-doped carbon materials from melamine, urea and dicyandiamide as nitrogen sources. The samples obtained with the addition of melamine and urea to the carbon materials demonstrated a high reversible specific capacity.

This work aimed to prepare highly-porous nitrogen-containing carbon materials from MFR using a solid template agent, nanocrystalline MgO, obtained in situ by thermal decomposition of magnesium citrate precursor added to the initial mixture. Obtained materials were characterized and their electrochemical properties – investigated.

2. Experimental

2.1. Initial reagents

Melamine $C_3H_6N_6$ (Reagent grade), 35% aqueous solution of formaldehyde HCHO (Khimprom, Novosibirsk, Reagent grade, 99,9%), dilute (0.01 M) NaOH water solution, concentrated water solution of hydrochloric acid HCl and distilled water were used as initial reagents. Magnesium citrate $Mg_3(C_6H_5O_7)_2{\cdot}10H_2O$ was prepared from citric acid and magnesium oxide as reported earlier [30].

2.2. Synthesis and characterization

Magnesium citrate powder was added to the water solution of melamine at the given weight ratios of the reagents $C_3H_6N_6$ and $Mg_3(C_6H_5O_7)_2{\cdot}10H_2O$ varying from 0 to 1. Then the formaldehyde solution was added to the obtained suspension in the molar ratio $C_3H_6N_6$:HCHO equal to 1:6, and the mixture was heated for an hour at a temperature of 75–80 °C and pH of 8–8.5. After the solution became viscous, the temperature was increased to 100 °C and kept at this temperature for 12 h until complete polymerization of the melamine-formaldehyde resin (MFR).

Pyrolysis was carried out in a tubular quartz reactor. The samples were placed in a nickel foil boat and heated in an inert argon atmosphere with a rate of 10 K/min up to 900 °C with 1 h dwell. The resulting composites containing carbon and the template agent were treated with HCl solution to remove the magnesium oxide which acted as a hard template. After treatment the samples were dried at 150 °C for 2 h for complete removal of residual moisture.

The resulting samples will be further designated as *L-x*, where *x* is the mass fraction of magnesium citrate in the initial magnesium citrate – melamine mixture. Figure 1 shows a schematic diagram of the synthesis process of nitrogen-containing carbon materials using melamine as a carbon and nitrogen source and magnesium citrate as a template agent precursor.

X-ray diffractograms of the samples were obtained on a Bruker D8 Advance diffractometer using Cu Kα (λ = 0.1542 nm) radiation in the 2θ angle range from 3° to 85°. The surface characteristics of the obtained carbon materials were evaluated using a nitrogen adsorption/desorption method at 77 K on a Termosorb TPD1200 surface analyzer. The total pore volume was determined from the adsorption value at P/P_0. The total surface area was estimated using the BET equation.

The surface of the obtained samples was examined using a "HITACHI TM1000" scanning electron microscope.

Raman spectra were recorded in backscattering geometry on a Senterra Raman microscope (Bruker, Germany) at room temperature with laser excitation (λ = 532 nm); the spectral measurement range was 500–3500 cm^{-1} with a resolution of 3–5 cm^{-1}.

X-ray photoelectron spectra (XPS) were recorded on a SPECS spectrometer (Germany) equipped with several isolated vacuum chambers for fast loading of samples, their thermal processing, and analysis.

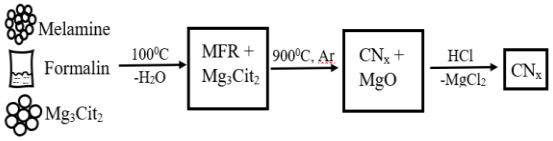

Figure 1 Schematic diagram of the process for producing nitrogen-containing carbon material.

 DOI: 10.15826/chimtech.2023.10.3.13

The samples for analysis were applied to double-sided conductive adhesive tape. The photoelectron spectra of the samples were recorded in the analyzer chamber at a pressure of $5 \cdot 10^{-9}$ Torr. The spectra were recorded for each sample using AlK ($h\nu$ = 1486.6 eV) radiation. The binding energy scale of the spectrometer was calibrated against the lines of metallic gold and copper, $Au4f_{7/2}$ = 84.0 eV and $Cu2p_{3/2}$ = 932.6 eV. The spectra of the samples were calibrated against the C1s line, the binding energy of which was assumed to be 284.8 eV.

The electrochemical studies were carried out in a two-electrode planar cell with two identical powder electrodes separated by a hydrophilic porous separator and placed in an electrolyte solution. The measurements by cyclic voltammetry were carried out using a potentiostat IPU-01 at the potential sweep rates of 5, 10, 20, 50 and 100 mV/s in solutions of 1 M H_2SO_4 and 3 M KOH. Galvanostatic charge-discharge curves were obtained on a device Analizator HIT Yarostanmash ACK2.5.10.8 (Russia) at a current density of 0.65 A/g in the voltage range from 0 to 0.8 V in M H_2SO_4. Impedance spectroscopy was carried out using Electrochemical Workstation ZIVE SP2 in the frequency range from 0.5 to 1 MHz in solutions of 1 M H_2SO_4.

3. Results and Discussion

3.1. X-Ray diffraction

The X-ray diffraction patterns of a composite prepared from the mixture of 30 wt.% melamine and 70 wt.% magnesium citrate by heat treatment at 900 °C in an inert argon atmosphere are presented in Figure 2. After the heat treatment at 900 °C the sample shows diffraction peaks corresponding to nanocrystalline MgO. The values of the grain size of magnesium oxide were estimated using a Scherrer equation:

$$d = \frac{K \cdot \lambda}{\beta \cdot \cos\theta}, \qquad (1)$$

where d is the grain size (or more correctly, the coherent domains size), λ is the X-ray wavelength (λ_{Cu} = 0.154 nm); θ is the diffraction reflections angle; K is the constant equal to 0.9. The estimation shows that the grain size of MgO in the composite is nearly 7 nm. After treatment of the composite with a solution of hydrochloric acid, all reflections attributed to magnesium oxide vanish due to a complete removal of the oxide from the resulting mesoporous carbon material. A strong low-angle X-ray scattering can be explained by the presence of mesopores in the carbon material under study.

3.2. Nitrogen adsorption studies

Figure 3 shows the dependence of the specific surface area on the mass fraction of magnesium citrate in the initial mixture. As can be seen from Figure 3, the product of pyrolysis of pure MFR has a small specific surface area. With an increase in the content of magnesium citrate in the initial mixture, the specific surface area of carbon materials increases and reaches a maximum value of 1304 m^2/g for pure magnesium citrate. The increase in the specific surface area occurs due to the increase in the content of nanocrystalline magnesium oxide, which, in turn, plays the role of a template agent responsible for the formation of pores in the final product.

However, despite the high specific surface area of the composite obtained from pure magnesium citrate, the product mass yield (i.e., the mass ratio of the pyrolysis product after MgO removal to the total mass of the carbon and nitrogen in the initial mixture) from this precursor is very small, around 4%. It is seen in Figure 4 which shows the mass yield of the carbon as a function of the magnesium citrate in the initial mixture.

One can see that the yield of the final carbon material depends on the mass content of magnesium citrate in the initial mixture. With the addition of magnesium citrate, the yield of the product increases and reaches a maximum at about 50–70% of magnesium citrate.

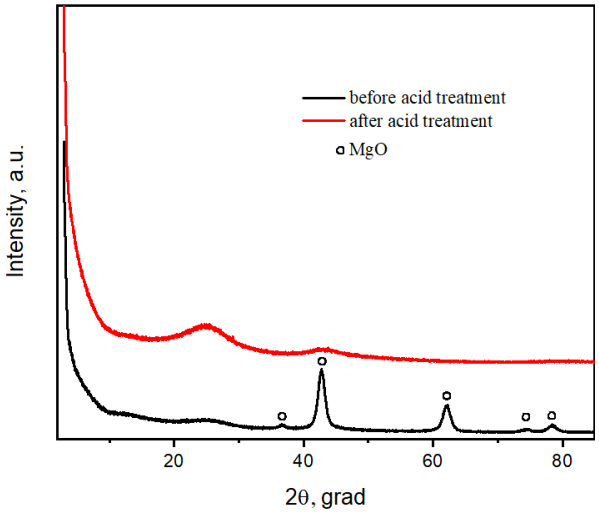

Figure 2 X-ray diffractogram of a L-70 composite containing 30 wt.% melamine and 70 wt.% magnesium citrate obtained by pyrolisis at 900 °C, before (black line) and after treatment with hydrochloric acid (red line).

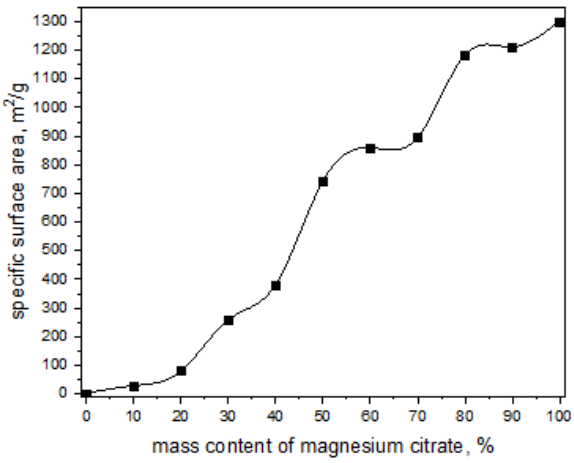

Figure 3 The variation of the specific surface area of the obtained materials on the content of magnesium citrate in the initial mixture.

 DOI: 10.15826/chimtech.2023.10.3.13

The reason for the decrease in the yield of carbon during the pyrolysis of MFR in inert atmosphere is the elimination of low molecular weight hydrocarbons and nitrogen-containing gases, such as ammonia, amines, etc., at high temperatures. Pyrolysis of pure MFR is accompanied by a nearly 90% weight loss. Magnesium citrate starts to decompose at relatively low temperatures with formation of amorphous phases of magnesium organic salts [30] and the escape of CO_2 and H_2O. At temperatures above 400 °C in inert atmosphere magnesium salts transform to nanocrystalline MgO and organic anions decompose with formation of highly-dispersed carbon and elimination of hydrocarbons and CO. As a result, the pyrolysis of pure magnesium citrate is accompanied by a nearly 95% weight loss. One would expect the mass yield of the final product to decrease from 11 to 4 wt.% with the increase in the magnesium citrate content in the initial compositions. Surprisingly, the dependence of the mass yield on the concentration has a strong maximum at 50–70 wt.% magnesium citrate in the initial mixture. The increase in the mass yield is important for practical applications. This effect requires additional, more detailed study and might be explained by an influence of the reaction of the magnesium citrate decomposition on the kinetics of the MFR pyrolysis.

3.3. Scanning electron microscopy

Morphology of the nitrogen-doped carbon materials was investigated using scanning electron microscopy (SEM); a typical SEM image is shown in Figure 5. It is seen that the sample consists of strongly aggregated particles of carbon material 3–10 μm in size. Each particle is a highly-porous pseudomorphosis of the initial polymeric matrix that retained its shape after the pyrolysis and subsequent acid treatment.

3.4. Raman and XPS spectroscopy data

The samples of nitrogen doped carbon were examined by Raman spectroscopy to determine the structure of the material. The Raman spectra are shown in Figure 6.

Peaks centered at 1340 cm^{-1} (including the unresolved D_3, D_1, and D_4 bands), 1600 cm^{-1} (including the unresolved G and D_2 bands), and 2680 cm^{-1} can be assigned to the D, G, and 2D bands, respectively. The presence of the D-band indicates the defectiveness of the material and also displays the degree of structural disorder. The D_3 band demonstrates a high intensity, indicating that the carbon materials are mainly amorphous. The G-band characterizes carbon bonds in the plane of the sp^2 vibrational mode; this parameter reflects the degree of crystallization of the material. The 2D band is related to the graphene layers in the material under study [31]. The presence of peaks at Raman shifts of 2680 cm^{-1} and 2940 cm^{-1} is caused by the presence of a small impurity of graphene-like fragments in the obtained material [32].

In order to investigate the nature of nitrogen atoms in the structure of the obtained materials, XPS spectra were recorded for the sample L-70. The spectra are presented in Figure 7. From the comparison of the intensities of C1s and N1s peaks it was found that the atomic ratio of N/C is equal to 0.04. This value is much lower than the stoichiometric N/C ratio in the initial compositions, which is equal to 0.67.

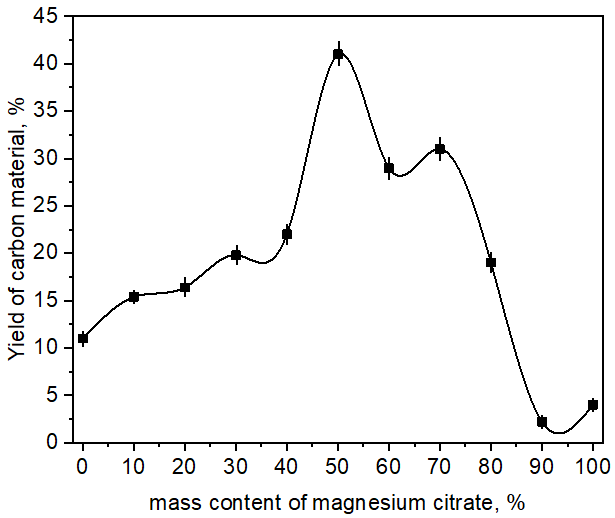

Figure 4 Mass yield of the carbon as a function of the magnesium citrate in the initial mixture.

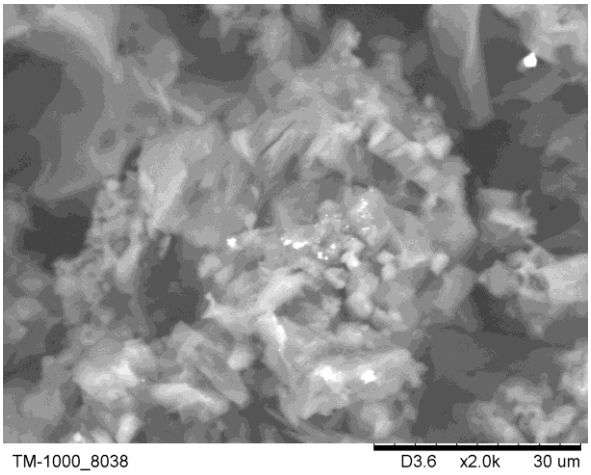

Figure 5 Scanning electron microscopy image of L-70 sample.

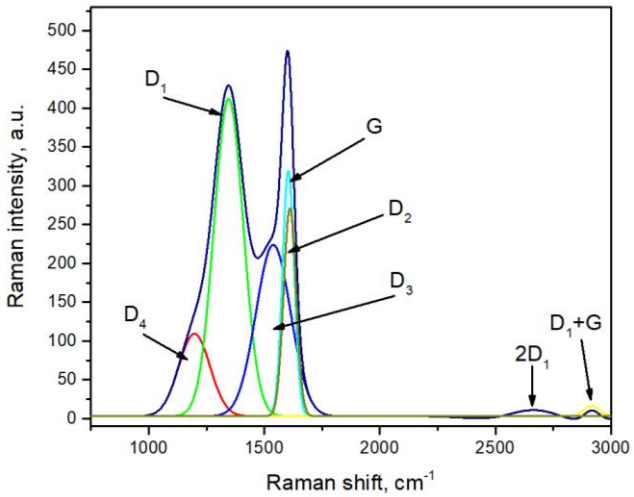

Figure 6 The Raman spectrum of L-70 sample and its decomposition into components (descriptions are given in the text).

 DOI: 10.15826/chimtech.2023.10.3.13

The main reason for the diminishing of the nitrogen content seems to be a relatively easy escape of nitrogen-containing products from the resin structure during the pyrolysis due to lower values of the binding energy of C–N bonds compared to C–C bonds.

The complex spectrum of the N1s region after deconvolution using the XPS Peak package can be described as a superposition of three peaks corresponding to the electronic states of nitrogen: pyridinic-N (398.2 eV); pyrrolic-N (400.3 eV); graphitic-N (or quaternary-N) (401 eV). Such spectra are typical of other nitrogen-doped carbon materials [33]. According to the qualitative analysis, the relative concentrations of pyridinic-N, pyrrolic-N and graphitic-N are 20%, 35% and 45%, respectively.

3.5. Electrochemical properties

3.5.1. Cyclic voltamperometry

To investigate the possibility of using the obtained N-doped carbon materials in supercapacitor applications, cyclic voltammogram (CVA) study was carried out using the samples under study as electrodes in symmetric cells with different electrolytes. Figure 8 shows the CVA curves obtained in acidic and basic electrolytes.

Specific capacitance per unit mass of carbon material C_m was calculated using the following formula:

$$C_m = \frac{1}{(U_2 - U_1) \cdot m \cdot v} \int_{U_1}^{U_2} I(t) dU, \qquad (2)$$

where I is the current value (A); U_1 and U_2 are the voltage limits between which the voltage scan is performed (V); v is the potential sweep rate (V/s); m is the total mass of carbon material on two electrodes (g).

Tables 1 and 2 show the results of voltammetry of the obtained series of samples in acidic and alkaline electrolytes at different potential sweep rates. The specific capacity of the samples in acidic electrolyte has a fairly high value, exceeding 100 F/g. It can also be observed that with an increase in the mass content of magnesium citrate in the initial mixture, the specific capacity increases, goes through a flattened maximum in the range from 30 to 90 wt.% magnesium citrate and strongly decreases for the sample L-100. Similar trend is observed for the capacitance values obtained in 3M KOH alkaline electrolyte. The comparison shows that the specific capacitance values obtained in an acidic electrolyte are 2–3 times higher than those obtained in an alkaline electrolyte.

It is known [34] that the specific capacitance of highly porous materials is defined by contributions of the double charge layer, C_{DL}, and the pseudocapacitance C_{ps}. The latter is the result of Faradaic effects, i.e. electrochemical processes proceeding on the electrodes which are defined by the diffusion of the reagents or products to the electrode surface and depends on the sweep rate. In order to separate the C_{ps} contribution into the overall capacitance, one can use the relation [35, 36]:

$$C_m = C_{DL} + \alpha \cdot v^{-1/2}, \qquad (3)$$

where the second term on the right-hand side corresponds to the contribution of the pseudocapacitance. According to Equation (2), the dependence of C_m on $v^{-1/2}$ should be linear, and the double layer capacitance C_{DL} can be found from the intersect ion of this curve with the C_m axis. Figure 9 shows such dependences for some nitrogen-doped carbon materials obtained in acidic and basic electrolytes.

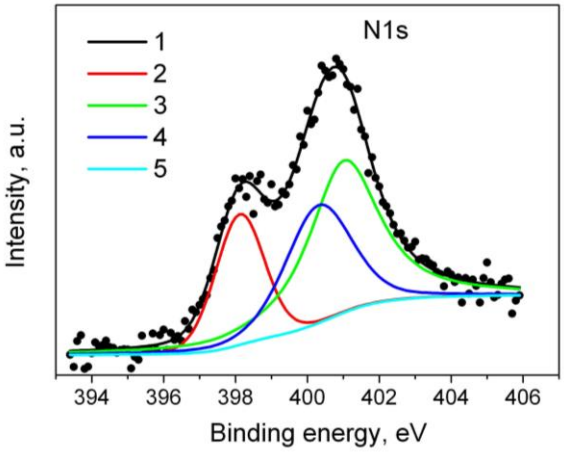

Figure 7 XPS spectra of N1s for L-70 sample. Points are experimental data, lines are calculated spectrum (1) obtained by superposition of contributions of pyridinic-N (2), pyrrolic-N (3), graphitic-N (4) and the background (5).

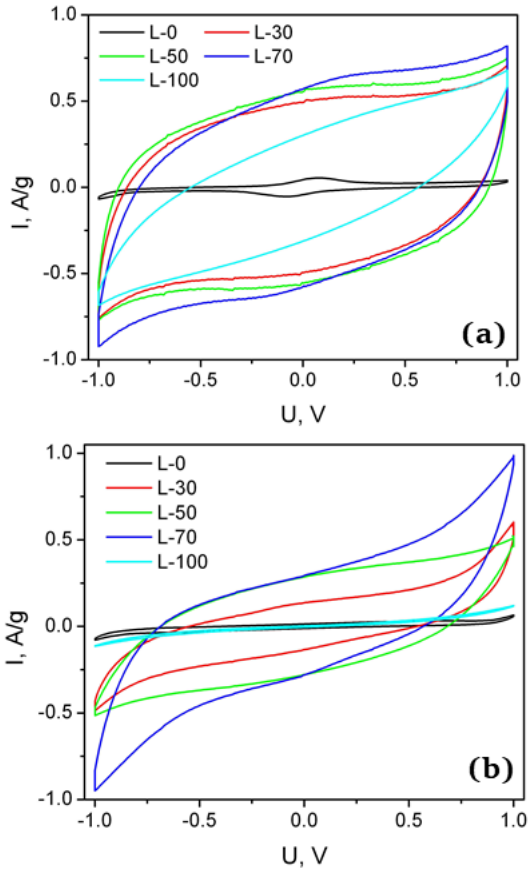

Figure 8 Cyclic voltammograms of the samples under study obtained for the samples under study in water solutions of 1 M H_2SO_4 (a) and 3 M KOH (b).

 DOI: 10.15826/chimtech.2023.10.3.13

Table 1 Specific capacity of the obtained samples at potential sweep rates of 5, 10, 20, 50 and 100 mV/s in 1 M H_2SO_4 electrolyte.

Sample	Specific capacity, F/g, at potential sweep rate, mV/s				
	5	10	20	50	100
L-0	10	10	6	3	1.8
L-10	56	50	40	30	20
L-20	71	55	42	29	20
L-30	111	100	95	75	52
L-40	117	108	88	65	48
L-50	120	112	108	82	64
L-60	121	120	114	96	60
L-70	118	115	111	81	58
L-80	120	119	97	69	46
L-90	110	108	119	91	63
L-100	61	47	56	30	18

Table 2 Specific capacity of the samples at potential sweep rates of 5, 10, 20, 50 and 100 mV/s in 3 M KOH electrolyte.

Sample	Specific capacity, F/g, at potential sweep rate, mV/s				
	5	10	20	50	100
L-0	5	3	1.6	1	0.6
L-10	22	24	23	22	20
L-20	26	24	20	16	12
L-30	32	28	24	16	12
L-40	60	54	28	22	16
L-50	62	58	40	25	10
L-60	61	55	34	24	14
L-70	64	60	54	43	32
L-80	66	65	57	44	35
L-90	15	12	8	4	2
L-100	1	0.8	0.4	0.1	0.08

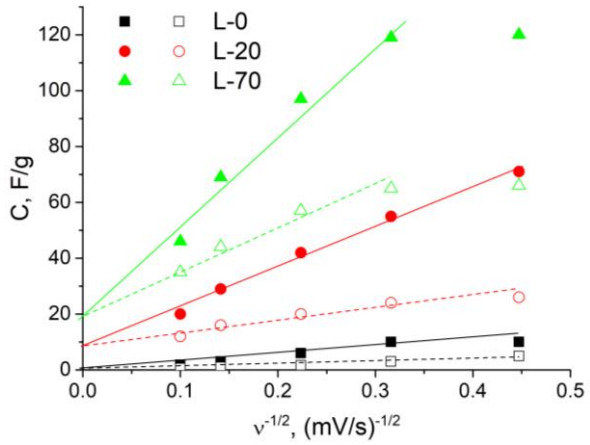

Figure 9 C_m vs $\nu^{-1/2}$ dependences for some samples under study: filled and open symbols are experimental data obtained in 1M H_2SO_4 and 3M KOH electrolytes, respectively, lines are linear dependences corresponding to Equation (2) for acidic (solid lines) and basic (dotted lines) electrolytes.

The analysis of the data shows that Equation (2) satisfactorily describes experimental data at the scan rates above 10 mV/s. The values of C_m obtained at smaller scan rates deviate from the theoretical dependence, and more sophisticated approaches should be used to explain this effect. Both contributions, C_{DL} and $C_{ps} \approx \alpha\nu^{-1/2}$, have maxima for L-70 sample. At low scan rates the pseudocapacitance gives the main contribution to the overall capacitance, whereas the maximum value of the double layer capacitance is less than 20 F/g. According to the data reported in the literature [34, 37], Faradaic processes in nitrogen-doped carbon materials are accompanied by the proton transfer. Therefore, C_{sp} values in acidic electrolytes are higher than in basic ones.

The maxima on the concentration dependences of C_{DL} and C_{ps} are caused by two factors: the increase in the specific surface area and the decrease in the total concentration of nitrogen in carbon materials. Both capacitances, C_{DL} and C_{ps}, are defined by the concentration of active surface centers. The estimation of the specific capacitance normalized per unit surface of the electrode material C_s [F/m²] using the equation

$$C_S = \frac{C_m}{S_{sp}}, \quad (4)$$

where S_{sp} [m²/g] is the specific surface area of the material, shows that the value of C_s in the samples under study depends on the electrolyte used and has a maximum of 0.10 F/m² for the L-80 sample. Comparison with the literature data shows that this value is lower than the pseudocapacitance values for nitrogen-doped carbon materials [37], which may be explained by a relatively low surface concentration of nitrogen in the samples under study. To increase this concentration, the pyrolysis should be done in the atmosphere of nitrogen or ammonia. Relatively low values of the double layer capacitance C_{DL} in the samples under study compared to the data reported for activated carbons [34, 38] seem to be caused by an influence of the surface nitrogen centers on the adsorption activity of adjacent carbon atoms. As a result, only a part of carbon atoms participates in the formation of the surface double layer, and the pseudocapacitance gives main contribution into total C_m and C_S values.

3.5.2. Galvanostatic chage-dicharge

The results of galvanostatic charge-discharge tests of sample L-70 at a current density of 0.65 A/g are shown in Figure 10. The curves have a symmetrical triangular type behavior, which indicates the terminal electrical capacitance of the double layer. A small hump can be observed on the charge and discharge curves, by which one can judge the presence of Faraday reactions, which are caused by the presence of heteroatoms in the structure [39]. The specific capacitance calculated from the discharge curve is 112 F/g, which is almost identical to the integrated area CV curves at the voltage sweep rates of 10 to 20 mV/s.

3.5.3. Impedance spectroscopy

The impedance plot obtained for the electrochemical cell is presented in Figure 11. The impedance data were successfully fitted by the equivalent circuit (see Figure 11) including the inductance contribution L due to the terminals, the resistance of the electrolyte, R_e, and the electrode impedance which consists of active resistance R_1 connected in parallel to the constant phase element $CPE_1 = Y1\cdot(i\omega)^{\alpha 1}$ and another constant phase element $CPE_2 = Y2\cdot(i\omega)^{\alpha 2}$.

 DOI: 10.15826/chimtech.2023.10.3.13

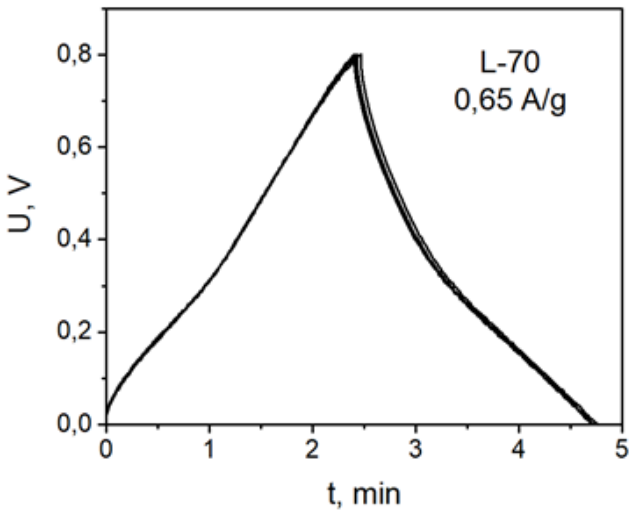

Figure 10 Galvanostatic charge-discharge curves of sample L-70 in water solutions of 1M H_2SO_4 at a current density of 0.65 A/g.

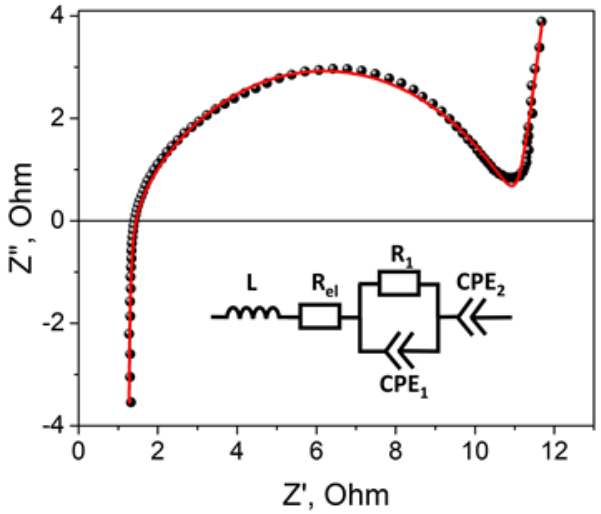

Figure 11 The impedance plot obtained for the electrochemical cell and the equivalent circuit used for the data interpretation. Points are experimental data, line is the fitting curve.

It was found that the resistances of the electrolyte Re and the electrode resistance R_1 are equal to 1.2 Ohm and 9.9 Ohm, respectively. Capacitance contributions are determined by CPE1 and CPE2 values, which are equal to $2.9 \cdot 10^{-4} \cdot (i\omega)^{0.68}$ and $8.1 \cdot 10^{-2} \cdot (i\omega)^{0.90}$, respectively. The exponent α_2 for CPE_2 contribution is close to unity. It means that the CPE_2 may be regarded as a slightly non-ideal capacitance (for which the parameter α should be equal to 1).

4. Limitations

This work demonstrated that solid template approach may be used for synthesis of highly-porous nitrogen-containing carbon materials from MFR. Nevertheless, many aspects of the work should be considered in more detail. To increase the nitrogen concentration in the materials under study the synthesis should be repeated in a nitrogen-containing atmosphere to minimize the nitrogen loss during pyrolysis. Other precursor salts could be tested as solid templates instead of magnesium citrate. Possibly, the use of other salts could allow one to increase further the mass yield of the carbon materials. In the present study we have discussed only the role of the specific surface area. In future, it would be desirable to investigate the influence of the pore size distribution on the properties of the materials. Electrochemical studies also require carrying out additional experiments aimed to establish correlations between concentration of the nitrogen, double layer capacitance and pseudocapacitance. Moreover, the decrease in the pseudocapacitance observed at low voltage sweep needs more thorough investigation and theoretical explanation.

5. Conclusion

In this work carbon materials doped with nitrogen were obtained for the first time by the hard template method followed by pyrolysis of melamine-formaldehyde resin (MFR). Nanocrystalline magnesium oxide used as a template agent was obtained by in situ thermolysis of magnesium citrate added to the melamine precursor. X-ray diffraction phase analysis revealed that the size of the resulting magnesium oxide is 7 nm and the carbon matrix is amorphous. By the method of BET nitrogen adsorption, the specific surface area of all samples was estimated, and it was found that with an increase in the content of magnesium citrate in the initial mixture the specific surface area of final carbon materials increases from 2 m^2/g for pure MFR to 1304 m^2/g for the pure magnesium citrate. The mass yield of carbon material depends on the magnesium citrate content in the initial mixture, and at 50–70 wt.% magnesium citrate it is several times higher than that in the materials obtained from pure components. According to the Raman spectroscopy and XPS spectroscopy data, the surface concentration of nitrogen is 4% and the carbon occurs mostly in an amorphous state with small amount of graphene fragments. The samples under study show excellent capacitance characteristics relative to their specific surface area. In 1 M of H_2SO_4, the specific capacity of the samples obtained from the precursors with a mass content of magnesium citrate from 30–90% exceeds 110 F/g. In 3 M KOH, the samples show lower values of specific capacity. The capacitance of the samples is mainly due to the contribution of the pseudocapacitance rather than the double layer capacitance in agreement with the earlier data for nitrogen-containing carbon materials [37]. Finally, it can be concluded that the materials obtained by the hard template pyrolysis of MFR are promising electrode materials for supercapacitors with aqueous electrolytes.

• Supplementary materials

No supplementary materials are available.

• Funding

The research was carried out with financial support within the framework of the NSTU development program, scientific project No. C23-31.

 DOI: 10.15826/chimtech.2023.10.3.13

• Acknowledgments

None.

• Author contributions

Conceptualization: Yu.S., N.U.
Data curation: Yu.S., N.U.
Formal Analysis: Yu.S., N.U.
Investigation: Yu.S., A.N.
Methodology: Yu.S., A.N., N.U.
Validation: N.F.
Visualization: Yu.S.
Writing – original draft: Yu.S.
Writing – review & editing: N.F.

• Conflict of interest

The authors declare no conflict of interest.

• Additional information

Author IDs:

Yuliya Sinelnikova, Scopus ID 57283350800
Alexander Nizovskii, Scopus ID 56962797600
Nikolai Uvarov, Scopus ID 26435747000.

Websites:

Novosibirsk State Technical University, https://en.nstu.ru/;

Institute of Solid State Chemistry and Mechanochemistry, SB RAS, http://www.solid.nsc.ru/en/;

Boreskov Institute of Catalysis, SB RAS, https://en.catalysis.ru/.

References

1. Lang JW, Kong LB, Liu M, Luo YC, Kang L. Asymmetric supercapacitors based on stabilized α-Ni(OH)$_2$ and activated carbon. J Solid State Electrochem. 2010;14:1533–1539. doi:10.1007/s10008-009-0984-1
2. Gao D, Liu R, Yu W, Luo Z, Liu C, Fan S. Gravity-induced self-charging in carbon nanotube/polymer supercapacitors. J Phys Chem C. 2019;123(9):5249–5254. doi:10.1021/acs.jpcc.8b11644
3. Wu Q, Xu YX, Yao ZY, Liu AR, Shi GQ. Supercapacitors based on flexible graphene/polyaniline nanofiber composite films. ACS Nano. 2010;4(4):1963–1970. doi:10.1021/nn1000035
4. Qu Y, Zhang X, Lü W. et al. All-solid-state flexible supercapacitor using graphene/g-C_3N_4 composite capacitor electrodes. J Mater Sci. 2020;55:16334–16346. doi:10.1007/s10853-020-05156-7
5. Wei H, Wang H, Li A, Li H, Cui D, Dong M, Lin J, Fan J, Zhang J, Hou H, Shi Y, Zhou D, Guo Z. Advanced porous hierarchical activated carbon derived from agricultural wastes toward high performance supercapacitors. J Alloys Compd. 2019. doi:10.1016/j.jallcom.2019.153111
6. Du J, Zhang Y, Wu H, Hou S, Chen A. N-doped hollow mesoporous carbon spheres by improved dissolution-capture for supercapacitors. Carbon. 2020;156:523–528. doi:10.1016/j.carbon.2019.09.091
7. Vijayakumar M, Santhosh R, Adduru J, Rao TN, Karthik M. Activated carbon fibres as high performance supercapacitor electrodes with commercial level mass loading. Carbon. 2018;140:465–476. doi:10.1016/j.carbon.2018.08.052
8. Yu J, Wang M, Xu P, Cho S-H, Suhr J, Gong K, Meng L, Huang L, Byun J-H, Oh Y, Yan Y, Chou T-W. Ultrahigh-rate wire-shaped supercapacitor based on graphene fiber. Carbon. 2017;119:332–338. doi:10.1016/j.carbon.2017.04.052
9. Ni G, Qin F, Guo Z, Wang J. Nitrogen-doped asphaltene-based porous carbon fibers as supercapacitor electrode material with high specific capacitance. Electrochimica Acta. 2019;33:135270. doi:10.1016/j.electacta.2019.135270
10. Wen Z, Wang X, Mao S, Bo Z, Kim H, Cui S, Lu G, Feng X, Chen J. Crumpled nitrogen-doped graphene nanosheets with ultrahigh pore volume for high-performance supercapacitor. Adv Mater. 2012;24(41):5610–5616. doi:10.1002/adma.201201920
11. Xie J-M, Zhuang R, Du Y-X, Pei Y-W, Tan D-M, Xu F. Advances in sulfur-doped carbon materials for use as anodes in sodium-ion batteries. New Carbon Mater. 2023;38(2):305–316. doi:10.1016/S1872-5805(22)60630-9
12. Wu Z-S, Tan Y-Z, Zheng S, Wang S, Parvez K, Qin J, et al. Bottom-up fabrication of sulfur-doped graphene films derived from sulfur-annulated nanographene for ultrahigh volumetric capacitance micro-supercapacitors. J Am Chem Soc. 2017;139(12):4506–4512. doi:10.1021/jacs.7b00805
13. Bondarde MP, Wadekar PH, Some S. Synthesis of sulfur doped carbon nanoparticle for the improvement of supercapacitive performance. J Energy Storage. 2020;32:101783. doi:10.1016/j.est.2020.101783
14. Gunasekaran SS, Gopalakrishnan A, Subashchandrabose R, Badhulika S. Single Step, direct pyrolysis assisted synthesis of nitrogen-doped porous carbon nanosheets derived from bamboo wood for high energy density asymmetric supercapacitor. J Energy Storage. 2021;42:103048. doi:10.1016/j.est.2021.103048
15. Wang L, Sun J, Zhang H, Xu L, Liu G. Preparation of benzoxazine-based N-doped mesoporous carbon material and its electrochemical behaviour as supercapacitor. J Electroanal Chem. 2020;868:114196. doi:10.1016/j.jelechem.2020.114196
16. Chae JE, Annaka K, Hong K, Lee S-I, Munakata H, Kim S-S, Kanamura K. Electrochemical characterization of phosphorous-doped soft carbon using single particle for lithium battery anode. Electrochimica Acta. 2014;130:60–65. doi:10.1016/j.electacta.2014.03.009
17. Patiño J, López-Salas N, Gutiérrez MC, Carriazo D, Ferrer ML, Monte F. Phosphorus-doped carbon–carbon nanotube hierarchical monoliths as true three-dimensional electrodes in supercapacitor cells. J Mater Chem. 2016;4:1251–1263. doi:10.1039/C7TA90286G
18. Wang D, Wang Z, Li Y, Dong K, Shao J, Luo S, et al. In situ double-template fabrication of boron-doped 3d hierarchical porous carbon network as anode materials for Li-and Na-ion batteries. Appl Surf Sci. 2019;464:422–428. doi:10.1016/j.apsusc.2018.09.035
19. Poornima BH, Vijayakumar T. Hydrothermal synthesis of Boron -doped porous carbon from Azadirachta Indica wood for supercapacitor application. Inorg Chem Comm. 2022;145:109953. doi:10.1016/j.inoche.2022.109953
20. Patiño J, López-Salas N, Gutiérrez MC, Carriazo D, Ferrer ML, del Monte F. Phosphorus-doped carbon–carbon nanotube hierarchical monoliths as true three-dimensional electrodes in supercapacitor cells. J Mater Chem. 2016;4:1251–1263. doi:10.1039/C5TA09210H
21. Zhang LL, Zhao XS. Carbon-based materials as supercapacitor electrodes. Chem Soc Rev. 2009;38:2520. doi:10.1039/B813846J
22. Candelaria SL,Garcia DD, Liua D, Cao G. Nitrogen modification of highly porous carbon for improved supercapacitor performance. J Mater Chem. 2012;22:9884–9889. doi:10.1039/C2JM30923H
23. Zou K, Deng Y, Chen J, Qian Y, Yang Y, Li Y, Chen G. Hierarchically porous nitrogen-doped carbon derived from the activation of agriculture waste by potassium hydroxide and urea for

high-performance supercapacitors. J Power Sources. 2018;378:579–588. doi:10.1016/j.jpowsour.2017.12.081
24. Li S, Fan Z. Nitrogen-doped carbon mesh from pyrolysis of cotton in ammonia as binder-free electrodes of supercapacitors. Microporous Mesoporous Mater. 2019;274:313–317. doi:10.1016/j.micromeso.2018.09.002
25. Cazetta AL, Zhang T, Silva TL, Almeida VC, Asefa T.Bone char-derived metal-free N- and S-co-doped nanoporous carbon and its efficient electrocatalytic activity for hydrazine oxidation. Appl Catal B Environ. 2018;225:30–39. doi:10.1016/j.apcatb.2017.11.050
26. Guan ZRX, Liu H, Xu B, Hao X, Wang ZX, Chen LQ. Gelatin-pyrolyzed mesoporous carbon as a high-performance sodium-storage material. J Mater Chem A. 2015;3(15):7849–7854. doi:10.1039/c5ta01446h
27. Cui H, Chen H, Guo Z, Xu J, Shen J. Preparation of high surface area mesoporous melamine formaldehyde resins. Microporous Mesoporous Mater. 2020;309:110591. doi:10.1016/j.mcromeso.2020.110591
28. Yuan Y. Preparation of nitrogen doped carbon materials and analysis of their electrochemical performance. Int J Electrochem Sci. 2022;17(8):220825. doi:10.20964/2022.08.19
29. Liu H, Deng Y, Mao J, Chen M, Hu J, Ju Z, Xing Z, Cao X. Characteristics and electrochemical performances of nitrogen-doped graphene prepared using different carbon and nitrogen sources as anode for lithium ion batteries. Int J Electrochem Sci. 2021;16(4):210459. doi:10.20964/2021.04.03
30. Sinelnikova YE, Uvarov NF. Synthesis of nanocrystalline magnesium oxide by thermolysis of magnesium citrate. Mendeleev Comm. 2022;23(5):697–699. doi:10.1016/j.mencom.2022.09.044
31. Bokobza L, Bruneel J-L, Couzi M. Raman spectroscopy as a tool for the analysis of carbon-based materials (highly oriented pyrolitic graphite, multilayer graphene and multiwall carbon nanotubes) and of some of their elastomeric composites. Vib Spectrosc. 2014;74:57–63. doi:10.1016/j.vibspec.2014.07.009
32. Tuinstra F, Coenig JL. Characterization of graphite fiber surface with Raman spectroscopy. J Compos Mater. 1970;4:492–499.
33. Jeon I-Y, Noh H-J, Baek J-B. Nitrogen-doped carbon nanomaterials: synthesis, characteristics and applications. Chem Asian J. 2020;15:2282–2293. doi:10.1002/asia.201901318
34. Béguin F, Raymundo-Piñero E, Frackowiak E. Electrical double-layer capacitors and pseudocapacitors. in: carbons for electrochemical energy storage and conversion systems. Taylor and Fransis LLC., 2010. Chapter 8. P.329–375. doi:10.1201/9781420055405-c8
35. Ardizzone S, Fregonara G, Trasatti S. “Inner” and “outer” active surface of RuO_2 electrodes. Electrochimica Acta. 1990;35(1):263–267. doi:10.1016/0013-4686(90)85068-X
36. Augustyn V, Simon P, Dunn B. Pseudocapacitive oxide materials for high-rate electrochemical energy storage. Energy Environ Sci. 2014;7:1597–1614. doi:10.1039/c3ee44164d
37. Frackowiak E, Lota G, Machnikowski J, Kierzek K, Vix C, Beguin F. Optimisation of supercapacitors using carbons with controlled nanotexture and nitrogen content. Electrochim Acta. 2006;51(11):2209–2214. doi:10.1016/j.electacta.2005.04.080
38. Centeno TA, Stoeckli F. The role of textural characteristics and oxygen-containing surface groups in the supercapacitor performances of activated carbons. Electrochimica Acta. 2006;52:560–566. doi:10.1016/j.electacta.2006.05.035
39. Li X, Zhang W, Wu M, Li S, Li XL, Li ZG. Multiple-heteroatom doped porous carbons from self-activation of lignosulfonate with melamine for high performance supercapacitors. Int J Biol Macromol. 2021;183:950–961. doi:10.1016/j.ijbiomac.2021.05.028

 DOI: 10.15826/chimtech.2023.10.3.13